



A Proof of Concept Balanced Mixer with the use of a Digital IF Power Combiner to Improve LO Noise Rejection

David Monasterio^{1,2} , Sebastian Jorquera¹ , Franco Curotto¹ , Camilo Espinoza² , Ricardo Finger¹, and Leonardo Bronfman¹ 

¹Department of Astronomy, Universidad de Chile Santiago, 7591245, Chile

²National Radio Astronomy Observatory, Charlottesville, Virginia, USA

Received 2023 August 30; accepted 2023 October 27; published 2023 December 7

Abstract

In this work we present a novel digital technique, that allows local oscillator (LO) noise cancellation using a digital power combiner in a balanced mixer receiver architecture. A theoretical analysis of the noise cancellation using the proposed technique is derived and a proof of concept experiment is made for the *Ku*-Band. This experiment includes the design and construction of a custom balanced mixer and an artificial noise source. Experimental results show a consistent noise temperature reduction in comparison with a full analog mixer, and in some cases reaching noise temperature levels similar to the receiver operating without the artificial LO noise.

Unified Astronomy Thesaurus concepts: [Astronomical instrumentation \(799\)](#)

1. Introduction

Local oscillator (LO) noise contribution is a significant concern in high sensitivity heterodyne receiver applications, particularly in millimeter and sub-millimeter wave radio-astronomy (Fujii et al. 2016). To achieve the desired LO frequency, high multiplication factor chains are employed, introducing additional noise that is downconverted to the intermediate frequency (IF) range. Consequently, the overall noise temperature of the system increases by an amount equal to the ratio of the LO power used to its signal-to-noise ratio (S/N; Bryerton et al. 2007).

To address this issue, balanced mixers are commonly utilized as the downconverter element due to their unique ability to cancel out LO noise (Robert 2007). However, in practice, analog components within the balanced mixer architecture exhibit amplitude and phase imbalances that restrict the cancellation of noise, allowing a fraction of the LO noise to be downconverted to the IF. In order to enhance the rejection of LO noise, we propose the implementation of digital calibration techniques used for astronomical receivers, such as sideband separating receivers (Finger et al. 2013) and orthomodal transducers (Alvear et al. 2016). These calibration methods utilize as working principle the measurement of imbalances of the analog hardware and applying a calibration factor to correct them in digital.

By improving the performance of the balanced mixer digitally, not only the receiver temperature can be reduced, but also the component cost, and the design time could potentially be lowered, as the calibrated mixer would more easily reach minimum requirements. By adopting digital calibration, costly cryogenic components could be replaced

by simpler room temperature ones, and older receivers with degraded performance could be recovered.

In this paper, we present the theoretical derivation of a digital noise cancellation method using a balanced mixer heterodyne receiver, outlining its assumptions and limitations regarding practical implementation. Additionally, we developed a proof-of-concept digital balanced mixer capable of reducing LO noise contribution to a greater extent than its analog equivalent. By using digital calibration techniques, we aim to mitigate the effects of amplitude and phase imbalances, ultimately improving the performance of heterodyne receivers in high sensitivity applications, especially where LO noise contribution becomes a significant factor.

2. Theoretical Derivation of Digital Noise Cancellation

2.1. Theoretical Derivation

The traditional balanced mixer architecture (Figure 1) consists of an input hybrid junction (90° or 180°) connected to two diodes with opposite orientations. The outputs of these diodes are combined using a power combiner into a single IF output that passes through a low-pass filter to eliminate the undesired frequencies. The main feature of this mixer configuration is that it eliminates, to a certain level, the LO noise that leaks to the IF. The fraction of LO that passes to the IF causes an increase in the system temperature, affecting the overall sensitivity of the receiver. In this section we will show the mathematics behind the LO noise rejection of the balanced mixer and the effect of the non-ideal components in limiting its performance.

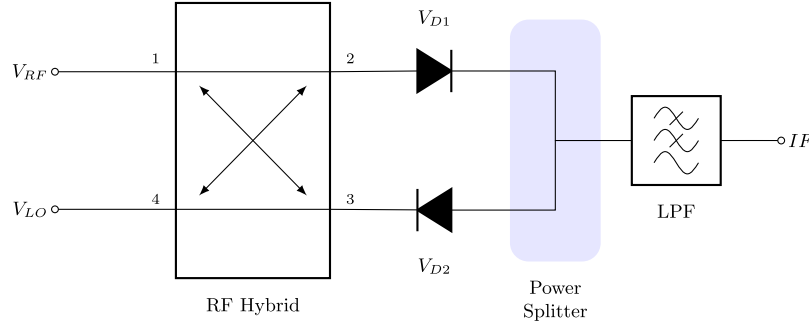


Figure 1. The traditional analog balanced mixer diagram.

A balanced mixer is a dual-sideband component, meaning that signals coming from the lower-side band (LSB) and upper-side band (USB) are both downconverted to the same IF. The dual-side band nature requires us to consider LO noise coming from both sidebands. For simplicity, we are going to treat the LO noise as harmonic signals that have a frequency $\omega_{lo} \pm \Delta$ added to the noiseless LO signal with frequency ω_{lo} . A similar approach has been used before in a multiple order analysis in Kheirdoost et al. (2009). For completeness we add a phase term in the noise terms, just to show that the phase term in an ideal balanced mixer will be canceled out and plays no role if the noise is coherent between the two branches.

These assumptions lead to Equation (1) to represent the LO signal and to Equation (2) that represents the RF signal, where $\nu_{usb} = \omega_{lo} + \omega_{usb}$ and $\nu_{lsb} = \omega_{lo} - \omega_{lsb}$.

$$V_{LO} = V_{lo} \cos(\omega_{lo}t) + \eta_{usb} \cos((\omega_{lo} + \Delta)t + \phi_{usb}) + \eta_{lsb} \cos((\omega_{lo} - \Delta)t + \phi_{lsb}) \quad (1)$$

$$V_{RF} = V_{usb} \cos(\nu_{usb}t) + V_{lsb} \cos(\nu_{lsb}t) \quad (2)$$

To study the effect of non-ideal components in the noise cancellation we add a deviation of the balanced mixer elements ideal response. In the hybrid this deviation is induced by adding a change in amplitude and phase to the ideal scattering parameters (Pozar 2008). This can be seen in Equation (3), where $|\mathcal{S}_{i,j}^{ideal}(\omega)| \angle (\phi_{i,j}^{ideal}(\omega))$ is the ideal response in magnitude angle notation and the term $|\hat{\mathcal{S}}_{i,j}(\omega)| \angle (\theta_{i,j}(\omega))$ corresponds to the deviation from the ideal behavior.

For the diodes we consider the standard Taylor series expansion to represent the nonlinear currents (Maas 2003), where each diode has its own coefficients set as Equations (4) and (5) show. Note that Equation (5) has a sign change in the terms due to the orientation of the diode in the architecture as Figure 1 depicts.

For the upcoming algebra, we are only interested in the quadratic terms with coefficients α_2 and β_2 . These terms produce the main downconversion for the RF signal and the LO noise if $\alpha_2 > \alpha_3 > \dots > \alpha_n$, which is a common assumption Robert (2007). Furthermore, in the subset of quadratic terms we only focus on the terms involving V_{lo} , because $V_{lo} \gg \eta_{usb}$,

η_{lsb} , V_{usb} , V_{lsb} so any second order expression that does not involve V_{lo} can be neglected.

$$\mathcal{S}_{i,j}^{non\ ideal}(\omega) = |\mathcal{S}_{i,j}^{ideal}(\omega)| \cdot |\hat{\mathcal{S}}_{i,j}(\omega)| \angle (\phi_{i,j}^{ideal}(\omega) + \theta_{i,j}(\omega)) \quad (3)$$

$$I_{D1} = \alpha_0 + \alpha_1 V_{D1} + \alpha_2 \frac{V_{D1}^2}{2} + \dots \quad (4)$$

$$I_{D2} = \beta_1 - \beta_2 V_{D2} + \beta_2 \frac{V_{D2}^2}{2} + \dots \quad (5)$$

Considering the previous assumptions and after some algebra, we arrive to the expressions for the diode's currents $I_{D1} = I_{D1,signal} + I_{D1,noise}$ and $I_{D2} = I_{D2,signal} + I_{D2,noise}$ given by Equations (6), (7), (8) and (9).

In the ideal case where $|\hat{\mathcal{S}}_{i,j}(\omega)| = 1$, $\theta_{i,j} = 0$ and $\alpha_2 = \beta_2$, it is generated the desired relation of $I_{D1,signal} = I_{D2,signal}$ and $I_{D1,noise} = -I_{D2,noise}$, so the addition of both diodes signals will eliminate the LO noise.

However, when the elements differ from the ideal condition, a portion of the LO noise is not perfectly eliminated and it passes to the IF, increasing the component noise temperature.

$$I_{D1,signal} = \alpha_2 [V_{lo} |\hat{\mathcal{S}}_{21}(\omega_{lo})| |\hat{\mathcal{S}}_{24}(\nu_{usb})| V_{usb} \times \sin(\omega_{usb}t + \theta_{24}(\nu_{usb}) - \theta_{21}(\omega_{lo})) + V_{lo} |\hat{\mathcal{S}}_{21}(\omega_{lo})| |\hat{\mathcal{S}}_{24}(\nu_{lsb})| V_{lsb} \times \sin(-\omega_{lsb}t + \theta_{24}(\nu_{usb}) - \theta_{21}(\omega_{lo}))] \quad (6)$$

$$I_{D1,noise} = \alpha_2 [V_{lo} |\hat{\mathcal{S}}_{21}(\omega_{lo})| (-|\hat{\mathcal{S}}_{21}(\omega_{lo} + \Delta)| \eta_{usb}) \times \cos(\Delta t + \phi_{usb} + \theta_{21}(\omega_{lo} + \Delta) - \theta_{21}(\omega_{lo})) + V_{lo} |\hat{\mathcal{S}}_{21}(\omega_{lo})| (-|\hat{\mathcal{S}}_{21}(\omega_{lo} - \Delta)| \eta_{lsb}) \times \cos(-\Delta t + \phi_{lsb} + \theta_{21}(\omega_{lo} - \Delta) - \theta_{21}(\omega_{lo}))] \quad (7)$$

$$I_{D2,signal} = \beta_2 [|\hat{\mathcal{S}}_{31}(\omega_{lo})| V_{lo} |\hat{\mathcal{S}}_{34}(\nu_{usb})| V_{usb} \times \sin(\omega_{usb}t + \theta_{34}(\nu_{usb}) - \theta_{31}(\omega_{lo})) + |\hat{\mathcal{S}}_{31}(\omega_{lo})| V_{lo} |\hat{\mathcal{S}}_{34}(\nu_{lsb})| V_{lsb} \times \sin(-\omega_{lsb}t + \theta_{34}(\nu_{lsb}) - \theta_{31}(\omega_{lo}))] \quad (8)$$

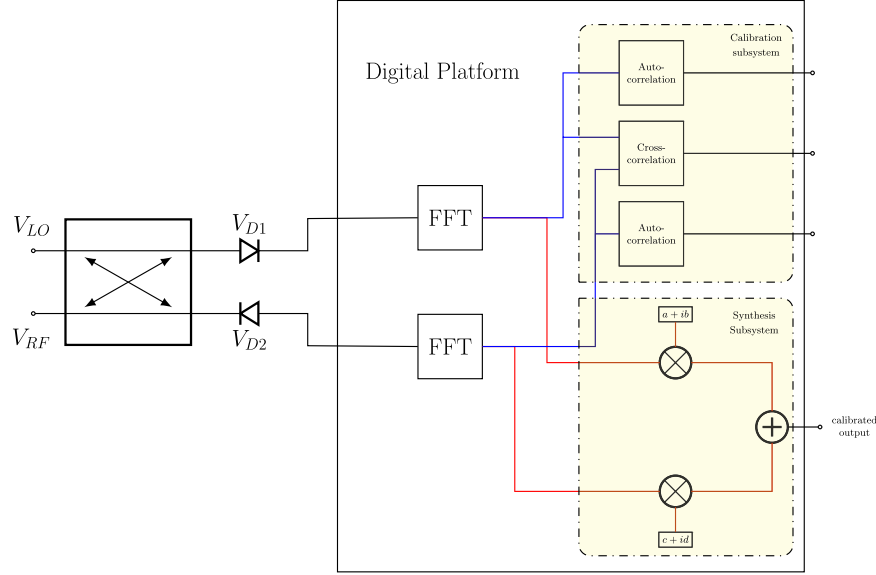


Figure 2. Digital system diagram.

$$\begin{aligned}
 I_{D2,\text{noise}} = & \beta_2 [|\hat{S}_{31}(\omega_{10})| |V_{10}| \hat{S}_{31}(\omega_{10} + \Delta) |\eta_{\text{usb}}| \\
 & \times \cos(\Delta t + \phi_{\text{usb}} + \theta_{31}(\omega_{10} + \Delta) - \theta_{31}(\omega_{10})) \\
 & + |\hat{S}_{31}(\omega_{10})| |V_{10}| \hat{S}_{31}(\omega_{10} - \Delta) |\eta_{\text{lsb}}| \\
 & \times \cos(-\Delta t + \phi_{\text{lsb}} + \theta_{31}(\omega_{10} - \Delta) - \theta_{31}(\omega_{10}))] \quad (9)
 \end{aligned}$$

As a solution to this LO noise leakage, inherent to the imbalances of the two diode's branches, we propose replacing the power combiner with a field programmable gate array (FPGA) platform to perform a weighted digital addition. This digital solution considers a calibration of the phase and amplitude of the signals coming from the diodes, reducing the imbalances in the mixer, thus increasing the noise rejection.

2.2. Calibration Method

The calibration method is based on the work of Finger et al. (2013) and Alvear et al. (2016). The authors replace the final IF component by a digital platform that is able to measure the imbalances of the analog system and correct them.

The firmware loaded into the digital platform comprises two subsystems (Figure 2):

1. A calibration subsystem which consists of an FX correlator in charge of measuring the analog system imbalances. This measurement enables the computation of a complex constant for each spectral channel that compensates for the imbalance.
2. A synthesis subsystem where the computed correction constants multiply the inputs and perform a complex addition to obtain the desired output.

In order to cancel the LO noise we need to achieve $I_{D1,\text{noise}} = -I_{D2,\text{noise}}$. This can be done by adding noise to the LO with an amplitude much larger than any RF signal during calibration. In this way the calibration measures only the imbalances in the LO path, and so the constants will be optimal to cancel the LO noise contribution.

Taking into account the previous requirement, the calibration constants are calculated using Equation (13) where the FX cross-correlation and auto-correlation are given by the expressions in Equations (10), (11) and (12), respectively. The expression in (13) satisfies $\boxed{\text{input D1}(i) \cdot \text{calibration constant} + \text{input D2} = 0}$ causing the rejection of the undesired signals.

$$\text{Cross - correlation}(i) = \text{input D1}(i) \cdot (\text{input D2}(i))^* \quad (10)$$

$$\text{Auto - correlation D1}(i) = \text{input D1}(i) \cdot (\text{input D1}(i))^* \quad (11)$$

$$\text{Auto - correlation D2}(i) = \text{input D2}(i) \cdot (\text{input D2}(i))^* \quad (12)$$

$$\text{Calibration constant}(i) = -\frac{\text{Cross - Correlation}(i)}{\text{Auto - correlation D2}(i)} \quad (13)$$

2.3. Calibration Limitations

The calibration procedure presented increases the noise rejection when compared with an analog balanced mixer, but the method has a fundamental limitation coming from the fact that the balanced mixer is a dual-sided band receiver. A dual side-band receiver downconverts LSB and USB to the same IF, as Equations (7) and (9) show. These LSB and USB terms got mapped to the cross-correlation and the auto-correlation, where

we can write them as an addition of functions that come from the LSB and USB as in Equations (14) and (15). The interpretation of this result is that the calibration constants are computed averaging the joint effect of noise from the LSB and USB in the IF as the expression in Equation (16) shows. This reduces, but not completely eliminates the LO noise.

Perfect LO noise cancellation may be possible by combining digital sideband separation with a digital balanced mixer, so that calibration can be applied at each sideband independently.

$$\text{Cross - correlation}(i) = A\{\text{USB}(i)\} + B\{\text{LSB}(i)\} \quad (14)$$

$$\text{Auto - correlation}(i) = C\{\text{USB}(i)\} + D\{\text{LSB}(i)\} \quad (15)$$

$$\begin{aligned} \text{Calibration constant}(i) &= -\frac{A\{\text{USB}(i)\} + B\{\text{LSB}(i)\}}{C\{\text{USB}(i)\} + D\{\text{LSB}(i)\}} \\ &= -\frac{A\{\text{USB}(i)\}}{C\{\text{USB}(i)\} + D\{\text{LSB}(i)\}} - \frac{B\{\text{LSB}(i)\}}{C\{\text{USB}(i)\} + D\{\text{LSB}(i)\}} \end{aligned} \quad (16)$$

3. Experiment Design

In this section we will present the analog components needed for the experimental validation of the proposed digitally compensated balanced mixer. These components include a specially balanced mixer without its final analog combiner, an artificial high-power noise source to simulate and control LO noise power, and finally a complete experimental test receiver. As the design frequency for the experiment, we selected the low part of the *Ku*-Band (12–16 GHz) as electronic components are commercially available for those frequencies.

3.1. Balanced Diode Mixer

The mixer was designed using Cadence[®] AWR Design Environment. The diodes selected for the design are Schottky Diode Skyworks part number SMS7621-040LF, which have good performance at the desired frequency range. We implemented the mixer using microstrip transmission lines with Rogers Duroid 4003 (0.508 mm thick) as its substrate.

The complete design layout is shown in Figure 3(b). A multistage branch-line coupler RF hybrid (Muraguchi et al. 1983) was selected for the design and RF shorts were used to control the RF reflections that pass through the diodes. Figure 3(a) shows the simulated characteristics of the designed hybrid. Notice that no special care was taken to optimize the hybrid in phase difference, as it is expected that the calibration to correct these errors. Discrete inductors connected in parallel at each IF branch were used as the diodes' DC drain. Several different types of simulators are included in AWR and were used for different parts of the design. All the linear components were designed and simulated using the AXIEM planar electromagnetic simulator, while the nonlinear heterodyne down-conversion was calculated using the Harmonic Balance (Maas 2003) APLAC simulator.

Simulation results, presented in Figure 3(c), show conversion losses of both IF outputs, at three different LO frequencies projected over the RF input. Both IF outputs show similar behavior over the entire IF range. The small discrepancies are produced by the amplitude imbalance of the RF hybrid. The conversion losses over the entire spectrum have an average value below 15 dB. This value considers the losses produced by the RF hybrid due to splitting the RF signal, so the actual conversion loss of the single-ended mixers is on average 3 dB lower. This value is consistent with the expected conversion losses using this type of diode. The increment of conversion loss near the LO frequency is a product of the DC drain circuit that acts as a high pass filter at very low frequencies (>10 MHz).

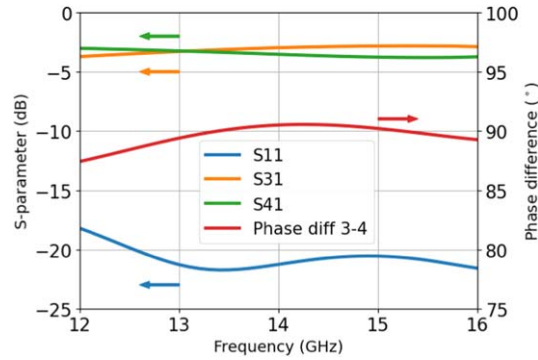
Characterization of the designed mixer follows the outline of Figure 4. The complete characterization of the conversion losses is obtained by changing the RF tone frequency as continuously as possible in the operating range of the mixer, for two different LO tones settings. These two LO tones are required to completely characterize the mixer over its operating bandwidth. An Anritsu MG3694C Signal Generator is used to provide the LO tone. The LO frequencies for this test are fixed either at 13 or 15 GHz depending on the measurement, with 6 dBm output power. The RF tone is generated by an Agilent E8257D PSG Analog Signal Generator, varying its output signal between 12 and 16 GHz at –20 dBm output power. Each IF output is characterized independently by connecting one to an Agilent N9000A CXA Signal Analyzer, while the other IF port is terminated in a matching load.

Figure 3(d) shows a photograph of the manufactured mixer. The PCB was made by using LPKF ProtoMat S43 and LPKF ProtoLaser S machines for drilling/cutting and copper-removal respectively. Southwest Microwave 292-05A-5 SMA Female End Launch Connectors were used for the RF and LO ports of this mixer. The discrete components (diodes and inductors), vias and IF output SMA connectors were hand-soldered.

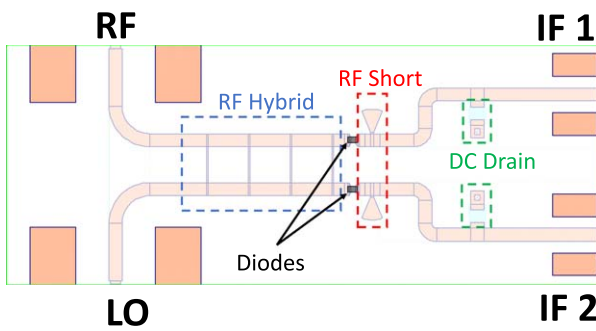
Figure 3(e) shows the measurement results for the conversion loss characterization. Note that curves are generated by sections because two LO tones were required to completely cover the bandwidth of the mixer. Both IF outputs have similar losses in the central part of the bandwidth, and differ from each other toward the lower and upper ends. This is mainly a contribution from the RF hybrid amplitude imbalance to the performance of the mixer. Also, an attenuation slope can be identified over the entire bandwidth. It was determined that this loss was produced by an increment in losses due to the manufacturing process.

3.2. LO Noise Source

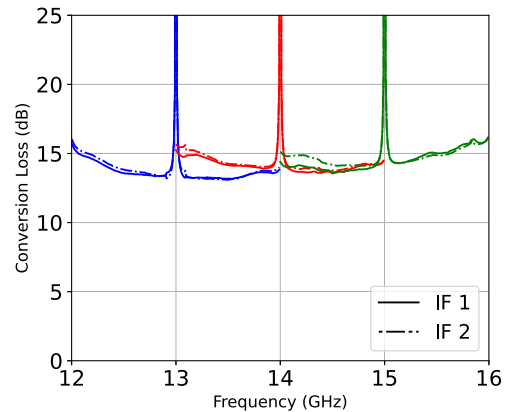
As the signal generators used for this experiment perform with minimum noise, an artificial LO noise source is required to control and study LO noise rejection. This source needs to



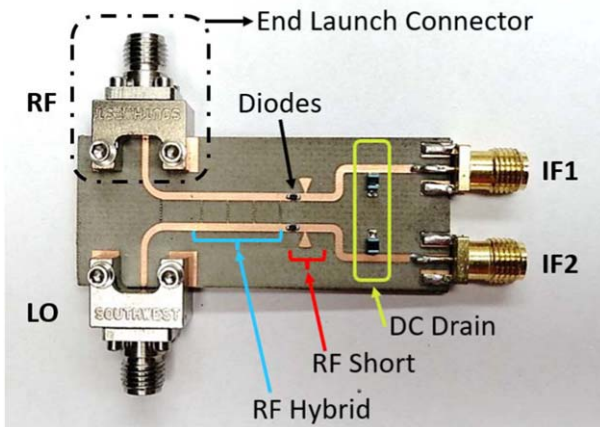
(a) Simulated characterization of RF hybrid.



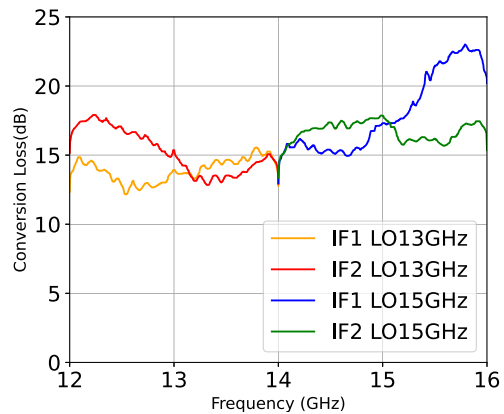
(b) Layout of the mixer.



(c) Simulated conversion loss for three LO settings: 13 GHz, 14 GHz and 15 GHz with 9 dBm of power.



(d) Photograph of the constructed mixer.



(e) Measured Conversion losses.

Figure 3. Balanced diode mixer.

inject enough noise power to ensure that LO noise can be measured, while avoiding saturation of the receiver. Figure 5 shows the setup to generate the artificial LO noise and the function of all its components. Several interchangeable passband filters were designed to cover different sections of

the *Ku*-Band. The designed filters consist of coupled line resonators implemented in microstrip line.

The resulting LO noise source is capable of generating considerable LO noise power over a limited bandwidth that is controllable. By using the filter presented in Figure 6(a), an

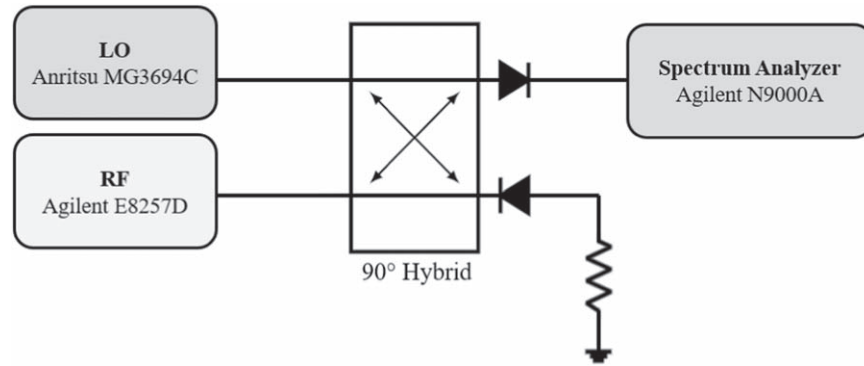


Figure 4. Setup for the characterization of conversion losses of the manufactured mixer. For simplicity, the mixer is represented as an RF hybrid and anti-parallel diodes only.

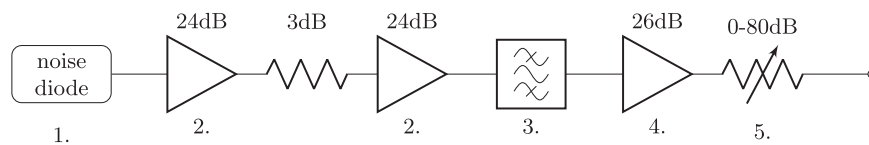
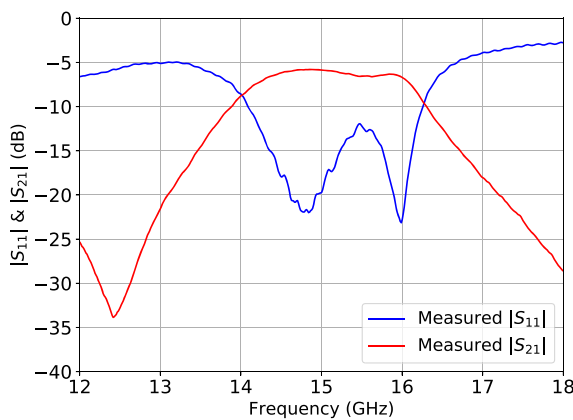
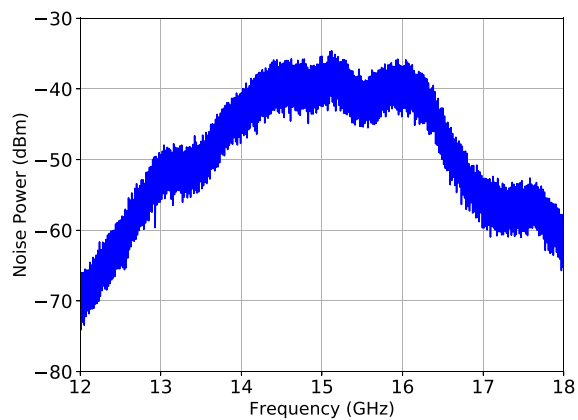


Figure 5. LO noise setup. The thermal noise is generated by an Agilent 346B noise source (1.). Then, the noise is amplified by two Minicircuits ZX60-183-S+ wideband microwave amplifiers (2.). Between the amplifiers, a 3 dB attenuator is placed to prevent ripple due to mismatch. To prevent saturation, LO noise must be injected only inside the band that is going to be downconverted, which can be done with the use of microwave filters (3.). At the output of the filter, a Minicircuits ZVA-183-S wideband amplifier (4.) with a high saturation point is placed to further increase the LO noise power. The Agilent 8945B and 8944B variable attenuator (5.) set is placed at the end of the setup to control the generated output LO Noise power and avoid receiver saturation.



(a) S parameters of the 15 GHz pass-band filter.



(b) Measured output noise power of artificial source.

Figure 6. Relevant measurements of the Artificial LO noise source. Noise measures were made utilizing an Agilent N9000A spectrum analyzer with a resolution bandwidth of 512 KHz.

example of the output LO power is presented in Figure 6(b) with 0 dB attenuation at the variable attenuator.

3.3. Complete Test Receiver Noise Measuring Setup

To validate the digital balanced mixer, we compared the performance of the mixer utilizing a digital and analog power combiner. As the figure of merit to compare both analog and

digital combiners, we decided to use the equivalent noise temperature of the receiver while using a noisy LO source.

To make these measurements, several other components needed to be included to have a fully functional test setup. Figure 7 presents the proposed setup. The Agilent 346B noise source used in the RF branch will be used with two settings. One is when the source is off (bias voltage of 0 V) and the load

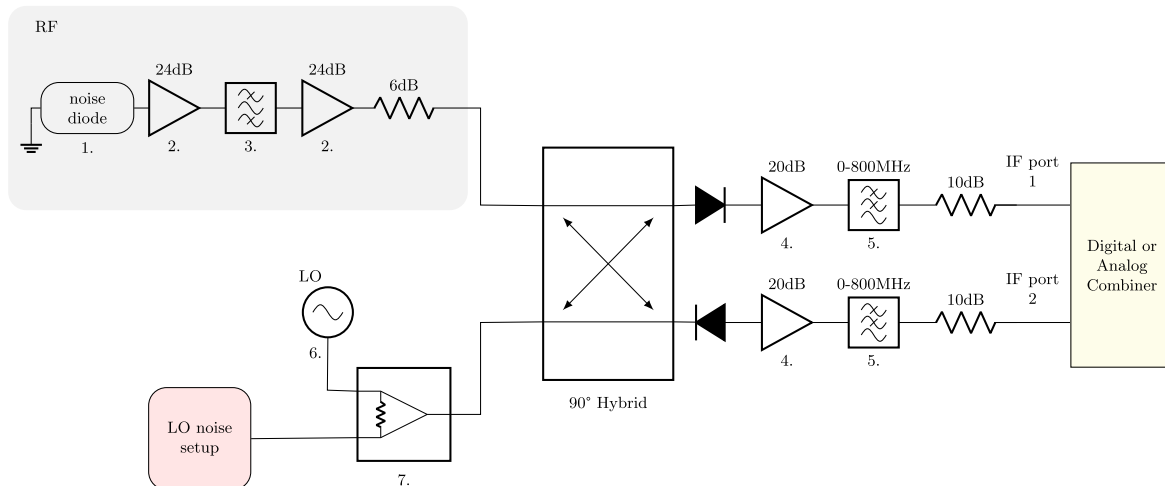


Figure 7. System diagram of the proposed test receiver. At the RF input of the receiver, an Agilent 346B noise source was placed (1.). Two Minicircuits ZX60-183-S + wideband microwave amplifiers are used to increase the RF receiver gain, needed to achieve the right sensitivity to measure noise temperature (2.). A 6 dB attenuator is placed at the output of the second amplifier to reduce any standing waves between the chain and the mixer. A bandpass filter is placed between the two RF amplifiers to reduce the noise contribution coming from the input load and avoid receiver saturation (3.). A Minicircuits ZX60-43-S+ amplifier is placed at each IF branch to increase receiver gain (4.). At the output of each IF amplifier, a coaxial low-pass filter is placed to eliminate undesired intermodulation products (5.), and to limit the LO noise that goes through the ADC into the digital back-end system. At the output of the filters, additional attenuation is placed to avoid ADC saturation. (5.) An Anritsu Signal Generator MG3694C was used as LO (6.). To combine the LO tone with the artificial LO noise a Minicircuits ZFRSC-183-S+ power splitter is used.

is at 290 K (ambient temperature). The other one is when the source is on (bias voltage of 28 V) and the load is at 9460 K (ENR of 15 dB). These two states are needed to apply the Y-factor method (Keysight Technologies 2021) and measure the noise temperature of the receiver.

Both IF ports 1 and 2 can be connected to either to the digital system where the digital combiner and spectrometer are implemented (as shown in Figure 2). Such ports can also be connected to an analog power combiner ZFSC-2-4, in which case, its output will be connected to a digital spectrometer. These two configurations will allow us to fully study the influence of the power combiner, as all other components of the setup will remain the same.

4. Experimental Results

4.1. Digital Calibration

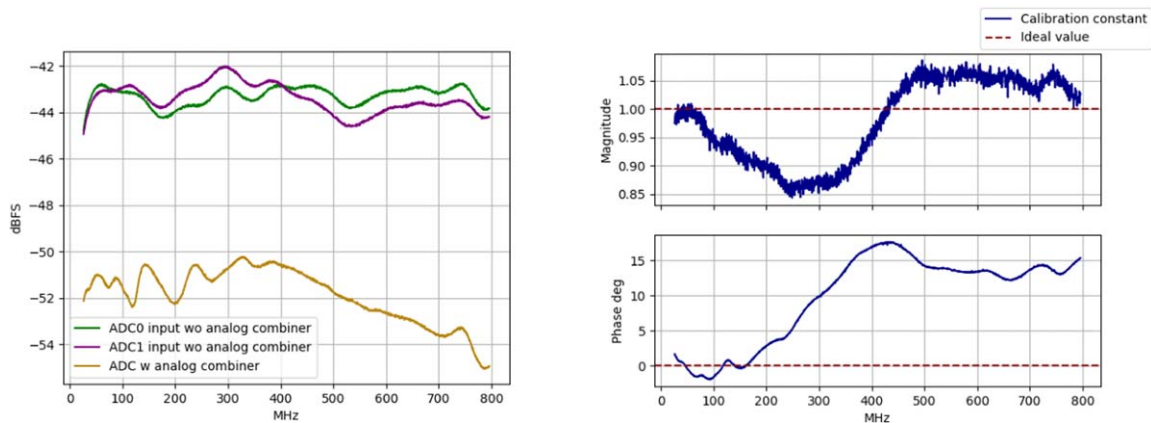
The selected platform for implementing the digital calibration stage was a ROACH2 developed by the CASPER group. The ROACH2 is composed of a Virtex6 FPGA where the correlator to measure the imbalances of the analog system and the calibrated combiner to correct the imbalances are implemented.

The ROACH2 platform is programmed with an FX correlator that uses a 2048 bin FFT with 1080 MHz of bandwidth, which yields a frequency resolution of 527.34 kHz. For the measurements, an average integration time of 60 ms was used. To calibrate, we used the noise signal coming from the LO as the calibration signal, averaging over the lower and

upper side-bands, as explained in Section 2.3. The digital balanced mixer noise cancellation has a conceptual limitation since USB and LSB got mapped to the same IF. For this, the use of a noise source is a good candidate to characterize the system as it will allow a good compromise for partial noise cancellation coming from both side-bands. In addition, as the noise is wideband it allows the simultaneous measurement of the imbalances for each channel, making the calibration process faster than using a generator injecting a frequency sweep in the band to characterize the system.

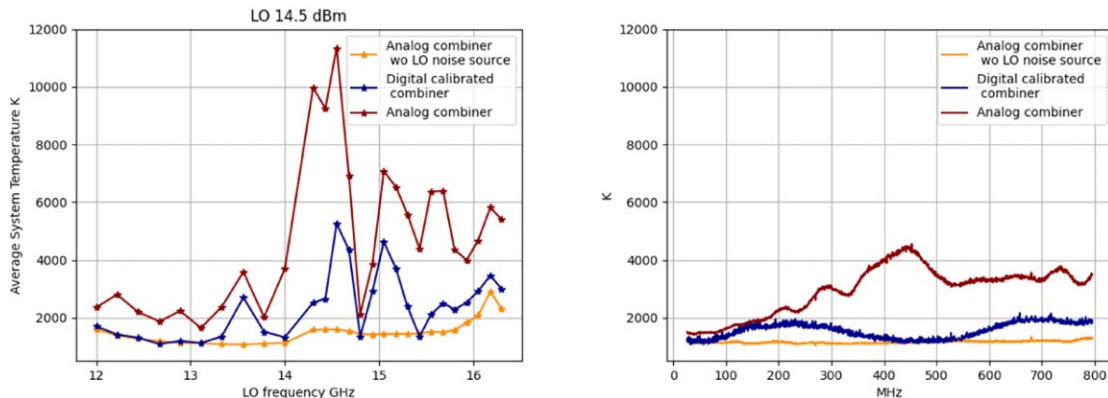
For each FFT channel for a given LO setting, we computed a complex correction factor after measuring the magnitude and phase imbalances so that the LO noise is minimized. As an example, we present in Figure 8(a) the ADC input power for both branches and in Figure 8(b) the calibration constants for each IF channel for an LO setting of 14 GHz. Results show the optimum amplitude and phase imbalance needed to minimize the LO noise contribution of the receiver. This example was selected because it shows a wide range of imbalances, with the lower frequencies up to 100 MHz showing values similar to an ideal combiner and significant amplitude and phase deviation at higher frequencies. This variation was produced by the non-ideal behavior of the components and connectors in each of the IF branches.

Figure 8(a) also shows that the total power received by the ADC is significantly larger with the digital combiner as compared to the analog case, where LO cancellation occurs in the analog combiner.



(a) IF power of both ADCs when doing calibration (top), (b) Complex calibration constants (solid blue) and ideal and total power received when utilizing an analog combiner (dashed red) used for an LO frequency of 14 GHz

Figure 8. Calibration measurements.



(a) Noise temperature of the receiver over the entire RF spectrum, averaged over 200 MHz of IF bandwidth (b) Noise temperature of the receiver over the entire IF spectrum, using a fixed LO of 14 GHz

Figure 9. Noise temperature measurements.

4.2. Noise Temperature Measurements

Noise temperature measurements were made for different LO frequencies, for both the analog and digital power combiners covering the entire RF spectrum (12–16GHz). We also measured the case without added LO noise source as a reference for the receiver performance. It is worth mentioning that even in that case there is some LO noise contribution coming from the Anritsu MG3694C synthesizer, but it is very low (< -145 dBm Hz^{-1} at offsets > 5 MHz from carrier as per instrument data sheet). Figure 9(a) shows the calculated noise temperature using a mobile LO with a fixed IF of 400 MHz with an integrated bandwidth of 200 MHz. Figure 9(b) shows an example of the noise temperature for a fixed LO of 14 GHz. Both results show that the receiver sensitivity is much better

when utilizing the digital calibrated combiner. For parts of the band performance of the digital mixer is as good as the analog mixer without LO noise. These results indicate that the receiver sensitivity is improved, eliminating the added noise produced by the noisy LO source as compared to its analog counterpart, thus making the receiver more robust to the variability of its components and to manufacturing errors. The results in Figure 9(b) also correlate with the calibration constants presented in Figure 8(b), showing similar behavior between the digital and analog cases when the calibration constants are similar to the ideal value and showing significant improvement when the difference is greater. However, the LO noise cancellation is not perfect for all the RF/IF bandwidth, as there are significant noise temperature differences between the

3 cases at several of the measured points. This behavior can be attributed to the limitation explained in Section 2.3.

Also, one particular phenomenon that requires attention is that at some points, the digital combination shows a slightly lower noise temperature value than the case without LO noise. This can be explained in two ways. First, by cancellation of the LO noise contribution coming from the synthesizer, since even in the absence of added noise, the LO source will have some broadband noise floor, of around -87dBc over spectral channel (527 kHz) at $>5\text{ MHz}$, computed using the generator technical information. Second, by a slight variation of the receiver noise temperature due to the different operating conditions when using an analog combiner and a digital combiner.

5. Conclusions

We have presented the theoretical derivation and experimental proof of concept of a Digital Balanced Mixer, that rejects LO noise using a digital power combiner in a balanced mixer architecture. An experimental receiver was built in the Ku band to demonstrate the technique.

Results show a consistent improvement in the receiver noise temperature as compared to the use of an analog combiner, particularly when the receiver possesses considerable noise coming from the LO.

The main limitation of the method is that the noise coming from the upper and lower sidebands can not be completely canceled simultaneously, but a compromise between them must be found. This effect produces different LO noise reduction for different LOs, but always a better performance than when using an analog combiner.

The calibration procedure is fast, since a broadband noise source is used, but special attention is required in order to avoid ADC saturation due to the added LO noise.

This method could prove as a viable alternative to decrease receiver noise temperature where the LO noise contribution is significant like in millimeter wave radio astronomy. The method could be also used to reduce mm-wave receiver complexity in cryogenic receiver, allowing the LO chain to be

put out of the cryostat, without compromising the receiver performance.

In future work, we aim to develop a more rigorous mathematical analysis to correctly characterize the limits of the technique. In addition, we plan to test the calibration in a state of the art receiver to measure if there are significant differences in performance when compared to unoptimized receivers.

Acknowledgments

R. Finger acknowledges the support of ANID through funds Basal FB210003, FONDECYT 1221662 and FONDEF ID21-10359.

ORCID iDs

David Monasterio  <https://orcid.org/0000-0002-6169-390X>
 Sebastian Jorquera  <https://orcid.org/0009-0001-2138-845X>
 Franco Curotto  <https://orcid.org/0000-0003-3261-2549>
 Camilo Espinoza  <https://orcid.org/0009-0002-4239-0134>
 Leonardo Bronfman  <https://orcid.org/0000-0002-9574-8454>

References

- Alvear, A., Finger, R., Fuentes, R., et al. 2016, *Proc. SPIE*, 9914, 99141E
 Bryerton, E. W., Morgan, M. A., Thacker, D. L., & Saini, K. S. 2007, in Proc. of 18th Int. Symp. on Space Terahertz Technology (Green Bank, WV: NRAO), 68
 Collin, R. E. 2007, *Foundations for Microwave Engineering* (2nd ed.; New York et al: Wiley)
 Finger, R., Mena, P., Reyes, N., Rodriguez, R., & Bronfman, L. 2013, *PASP*, 125, 263
 Fujii, Y., Kojima, T., & Gonzalez, A. 2016, *SuScT*, 30, 024001
 Keysight Technologies 2021, Noise Figure Measurement Accuracy: The Y-Factor Method 5952-3706
 Kheirdoost, A., Banai, A., & Farzaneh, F. 2009, *ITMTT*, 57, 760
 Muraguchi, M., Yukitake, T., & Naito, Y. 1983, *ITMTT*, 31, 674
 Pozar, D. M. 2008, *Microwave Engineering* (2nd ed; New York et al: Wiley)
 Maas, S. A. 2003, *Nonlinear Microwave and RF Circuits* (2nd ed.; Boston, MA: Artech House Publishers)